Since January 2020 Elsevier has created a COVID-19 resource centre with free information in English and Mandarin on the novel coronavirus COVID-19. The COVID-19 resource centre is hosted on Elsevier Connect, the company's public news and information website.

4.3 Nanomechanical Sensors

Kota Shiba*, Gaku Imamura*, Genki Yoshikawa**

*INTERNATIONAL CENTER FOR YOUNG SCIENTISTS (ICYS) & INTERNATIONAL CENTER FOR MATERIALS NANOARCHITECTONICS (MANA), NATIONAL INSTITUTE FOR MATERIALS SCIENCE (NIMS), TSUKUBA, JAPAN; **INTERNATIONAL CENTER FOR MATERIALS NANOARCHITECTONICS (MANA), NATIONAL INSTITUTE FOR MATERIALS SCIENCE (NIMS), TSUKUBA, JAPAN

CHAPTER OUTLINE

4.3.1 Introduction

Development of sensing technologies applicable to diverse biological species has been demanded for decades to realize a wide range of applications such as efficient drug screening, point-of-care testing, and early stage/noninvasive diagnostics, etc. To fulfill this demand, various kinds of sensors have been proposed so far. Among such sensors with different working principles, nanomechanical sensors have attracted much attention because of their remarkable features; high sensitivity, wide target range from small molecules to macromolecules, compatibility with industrial technologies, and so on [1]. A number of biological species such as viruses, proteins, bacteria, and cells have been investigated by means of nanomechanical sensors [2].

In this chapter, we will briefly review the basics of nanomechanical sensors, focusing on a microcantilever, which is known as a representative geometry of nanomechanical sensors. In addition to the conventional cantilever, a nanomechanical sensor with a membrane-type geometry will be highlighted as a newly developed sensing platform with various notable features [3–5]. Since affinity of sensors to sensing targets is affected by the type of functional layers, so-called "receptor layers," coated onto the sensor surface, it is important to properly design receptor layers depending on applications. Therefore, we will also discuss a strategy to realize an optimized receptor layer in terms of sensitivity and selectivity. Finally, the biological species measured by nanomechanical sensors will be summarized.

4.3.2 Nanomechanical Sensors

4.3.2.1 General Remarks

A nanomechanical sensor is a mechanical structure that transduces analyte-induced stimuli into a signal via its structural change with nanometer precision. The definition of a nanomechanical sensor can also cover a mechanical transducer with nanometer scale. In either sense, a cantilever sensor is a representative example among various geometries.

The first chemical sensing application using a cantilever sensor was demonstrated by Gimzewski et al. in 1994. They revealed that the static bending of a cantilever can be used as a calorimeter, which can detect the catalytic reaction taking place on the surface of a cantilever [6]. In the same year, Thundat et al. demonstrated a mass detection with picogram resolution using a cantilever. They focused on the shifts in cantilever resonance frequency induced by the exposure of a metal-coated cantilever to humidity or vapors of mercury [7]. Then, the target of cantilever sensors expanded to various phenomena, such as the formation of self-assembled monolayers [8] and the hybridization of DNA [9].

As demonstrated by various groups, nanomechanical sensors are applicable to a wide variety of targets. To take advantage of their attractive feature, it is important to understand the basics of nanomechanical sensors. In the following sections, we will briefly review working principles and readout methods of cantilever sensors [10]. Then, recent developments in the field of nanomechanical sensing will be highlighted.

4.3.2.2 Operation Modes

Cantilever sensors can detect the following two physical parameters: volume and/or mass of target molecules. Since all substances have volume and mass, we can measure almost any kind of substance by using cantilever sensors. To measure volume and mass of target molecules, there are basically two operation modes of cantilever sensors: static mode and dynamic mode (Fig. 4.3.1). Details will be described in the following sections.

4.3.2.2.1 Static Mode

The static mode is known as one of the representative operation modes of cantilever sensors; it measures surface stress, which is not easily measured with other sensing techniques. The major advantage of the static mode is that a cantilever is not affected by damping because the bending motion caused by the analyte-induced surface stress is slow enough, minimizing the damping in most cases. Since the damping of liquid media severely decreases the sensitivity in the dynamic mode, the static mode is a better option for measurements in a liquid environment. It does not require any complicated peripheral devices, such as actuators or high-frequency readout setups, which are usually necessary for dynamic mode measurements.

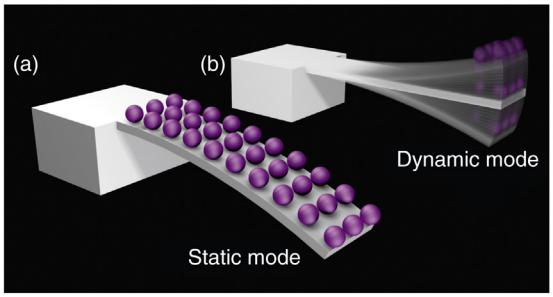

FIGURE 4.3.1 Schematic illustrations of (a) static mode and (b) dynamic mode operations. It is important to note that the bending of a cantilever is caused by the adsorbate-induced surface stress in the case of static mode (the gravity effect is almost negligible). *Reproduced from Ref. [10], with permission from the Royal Society of Chemistry.*

However, there are several issues to be addressed in static mode operation. The long-standing issue is the difficulties in interpreting obtained signals. At present, there is no well-accepted consensus on the origin of surface stress. Although it is roughly regarded as a result of an increase in electrostatic or steric interactions between the adsorbed analytes on the surface of a cantilever, a comprehensive model is still missing. Even for a model system of alkanethiols on a gold (111) surface, several explanations have been reported so far. Thus, the proper calibration should be performed for each application before the actual measurements.

For solid coating layers, a simple analytical model is proposed. It provides general reference values in terms of the strain induced in the coating layer [11,12]. It will help toward analyzing the static behavior of cantilever sensors and various nanomechanical sensors in conjunction with physical properties of coating films as well as optimizing the films for higher sensitivity. The details of the analytical model will be discussed later.

Another difficulty in the interpretation of a signal is the time-dependent complicated behavior, especially in the cases of polymer coatings [13] possibly due to viscoelastic effects [14].

4.3.2.2.2 Dynamic Mode

The concept of dynamic mode operation is same as that for various resonators, such as a quartz crystal microbalance. In this mode, the resonance frequency shift is measured. This shift is due to the change in effective mass induced by the adsorption of analytes on a cantilever. Since signals can be directly correlated to the basic property of adsorbates, that is, mass, the dynamic mode is a useful and powerful technique to derive quantitative information. As the sensitivity generally depends on the resonance frequency determined by the size of a cantilever, a nanometer scale cantilever operated at very high frequency bands (~30~300 MHz) marked several milestones, such as ~7 zeptogram (10^{-21} g) resolution (equivalent to ~30 xenon atoms) in a cryogenically cooled, ultrahigh vacuum (below 10^{-10} torr) apparatus [15], and the mass resolution less than 1 attogram (10^{-18} g) in air at room temperature [16].

The induced mass change (Δm) for a rectangular cantilever with the length of l, thickness of t, width of w, and Young's modulus of E, can be calculated by the following Eq. (4.3.1):

$$\Delta m = \frac{k}{4\pi^2} \times \left(\frac{1}{f_1^2} - \frac{1}{f_0^2} \right) \tag{4.3.1}$$

where $k = Ewt^3/(4l^3)$ is a spring constant of the cantilever, and f_0 and f_1 are the eigenfrequencies before and after the mass change. This equation is derived through pure mechanics, assuming the ideal condition. Thus, in practical situations, several issues still remain. One of the most important issues is the damping effect induced by the surrounding media, as briefly described in the previous section. The damping severely lowers the performance of a cantilever sensor in terms of a low quality factor Q, especially in a liquid environment where Q becomes one-tenth of that in air, resulting in low resolution to track the resonance frequency. Braun and Ghatkesar et al. proposed and demonstrated an elegant way to circumvent the damping effect in a liquid environment using higher flexural modes [17–19]. They succeeded in detecting protein–ligand interactions in a physiological environment at a sensitivity of 2.5 pg/Hz [17], and demonstrated the significant improvement in quality factor of up to ~30 times with the 16th flexural mode [19].

Other factors affecting the signals in the dynamic mode are adsorption-induced effects, such as surface stress and position dependence, which can either stiffen or soften the cantilever, thereby varying the spring constant. The relationship between the surface stress and stiffness of a cantilever has been intensively discussed [20–22]. Lee et al. visually demonstrated the dependence of resonance frequency on a pattern of a gold layer on the surface of a cantilever [23]. In any case, we have to be careful about these effects when we analyze the signals obtained with the dynamic mode.

4.3.2.3 Readout Methods

There are several readout methods to record responses of cantilever sensors [1]. In this section, we will introduce two representative readout methods: optical readout with a laser and electrical readout with a piezoresistor.

4.3.2.3.1 Optical Readout

The most commonly used readout method is the so-called optical readout, which utilizes laser light emitted from, for example, a vertical cavity surface emitting laser (VCSEL). The laser is reflected on the surface of a cantilever and then the position is measured by a position-sensitive detector (PSD) (Fig. 4.3.2). It gives high sensitivity in terms of signal-to-noise ratio because of its relatively low noise. Another practical advantage of this method is that there is no requirement for wiring on a cantilever array sensor chip because both the source and detector of laser light are placed at remote positions.

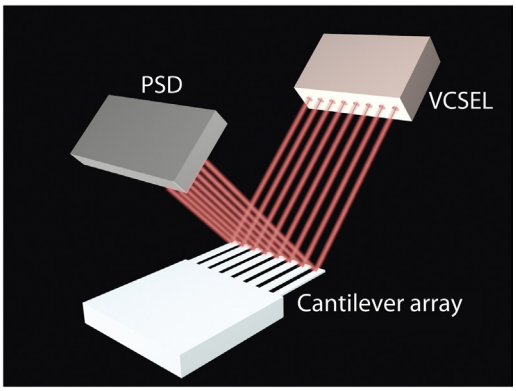

FIGURE 4.3.2 Typical setup for the optical (laser) readout system. VCSEL is usually used as a source of multiple laser light. Each laser light reflected on the surface of each cantilever is measured by a PSD. *Reproduced from Ref. [10], with permission from the Royal Society of Chemistry.*

However, optical readout has several drawbacks when we consider actual applications. First of all, laser-related peripherals are bulky and expensive in most cases. For multiple cantilevers such as a cantilever array, the same number of laser sources must be prepared. While highly integrated VCSEL or multiple optical fiber systems might be able to solve this problem, each laser light should be always aligned on each cantilever precisely. Thus, optical readout is not suitable for large one- or two-dimensional arrays. Another critical problem is the difficulty in measurements in opaque liquids, such as blood. In such a liquid, the optical signal is significantly attenuated owing to low transmission or refractive index change.

4.3.2.3.2 Piezoresistive Readout

Piezoresistive readout can be utilized by using a piezoresistive cantilever, in which a sensing element (piezoresistor) is embedded at the clamped end; thereby it is sometimes called a "self-sensing" cantilever (Fig. 4.3.3). In contrast to the optical readout method, no bulky and complex peripherals are required because a piezoresistive readout electrically measures the change in resistance of a piezoresistor with a simple circuit (Fig. 4.3.4). By means of the piezoresistive readout, it is also possible to perform measurements even in

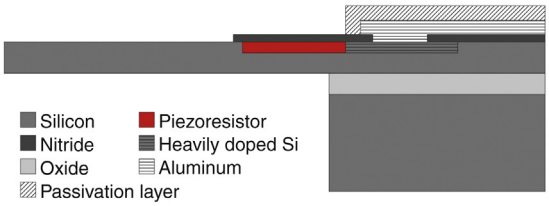

FIGURE 4.3.3 An example of the cross-section of a piezoresistive cantilever. It is important to cover the piezoresistor with a passivation layer, such as silicon nitride, to prevent leakage of current, especially in the case of measurements in a liquid environment. *Reprinted from Ref. [24], with permission from Elsevier B.V.*

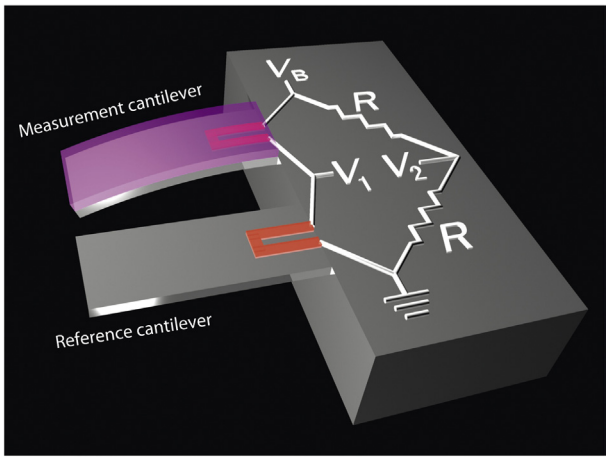

FIGURE 4.3.4 An example of electrical wiring of a piezoresistive readout. In this configuration, the differential signal is given as an output of the Wheatstone bridge, while it is also possible to place measurement and reference cantilevers in individual Wheatstone bridges and obtain differential signals by subtracting the output of the reference lever bridge from that of measurement lever bridge. *Reproduced from Ref. [10], with permission from the Royal Society of Chemistry.*

opaque liquids. In addition, because of its complementary metal-oxide semiconductor compatibility, the whole sensor unit including readout parts can be integrated into common semiconductor devices, such as mobile phones. It is also technically feasible by mass production to produce inexpensive disposal chips, which are important for various applications, especially for medical diagnosis. Thus, the piezoresistive readout has been regarded as one of the most promising approaches to overcome the problems arising from the optical readout. In spite of these inherent advantages, piezoresistive cantilevers have not been widely utilized for sensing applications because of their critically low sensitivity. In other words, they will open the door to the applications of nanomechanical sensors if the sensitivity of a piezoresistive cantilever can be significantly improved. Therefore, various trials have been made for more than a decade to improve the sensitivity of a piezoresistive cantilever toward practical uses. However, significant improvement in sensitivity has not been achieved to make piezoresistive detection comparable to the optical approach.

4.3.2.4 Structural Optimization of Nanomechanical Sensors for Improved Sensitivity

Various strategies have been proposed to improve the sensitivity of a piezoresistive cantilever by structural modification, such as making a through-hole [25,26], patterning of the cantilever surface [27], or variation of geometrical parameters (e.g., length, width, and overall shapes) [28,29]. Although these approaches gained some improvements in sensitivity (typically, a few tens of a percent, while up to ~5 times in some cases [29]), significant enhancement has not been achieved.

To realize the appropriate scheme for the enhanced sensitivity, it is important to note the basic properties of a piezoresistive cantilever for surface stress sensing [3]. One notable parameter is piezocoefficient. P-type piezoresistors created by boron diffusion onto a single-crystal silicon (100) surface can be effectively utilized because of its high piezocoefficient [30–32]. Plain stress (i.e., $\sigma_z = 0$) is assumed because of the intrinsically two-dimensional feature of surface stress. In this case, relative resistance change can be described as follows [32,33]:

$$\frac{\Delta R}{R} \approx \frac{1}{2}\pi_{44}(\sigma_x - \sigma_y) \tag{4.3.2}$$

where $\pi_{44}(\sim 138.1 \times 10^{-11}\ \mathrm{Pa}^{-1})$ is one of the fundamental piezoresistance coefficients of the silicon crystal. σ_x, σ_y, and σ_z are stresses induced on the piezoresistor in the [110], [1-10], and [001] directions of the crystal, respectively. Based on this equation, both enhancement of σ_x (σ_y) and suppression of σ_y (σ_x) are required to yield a substantial amount of $\Delta R/R$. However, in the case of surface stress sensing, the stress is basically isotropic. In other words, σ_x is almost equal to σ_y, resulting in $\Delta R/R \sim 0$. Therefore, the resultant signal is virtually zero on the whole surface. Because of this intrinsic material property, it is difficult to significantly improve sensitivity as long as we consider simple cantilever-type structures.

Through a detailed structural investigation, a new geometry with high sensitivity was developed. This structure is called a membrane-type surface stress sensor (MSS, Fig. 4.3.5a) [3]. In addition to the geometry, MSS was also optimized in terms of electric circuit. For p-type silicon (100), the relative resistance change with a current flow in the x-direction is given by Eq. (4.3.2). In case all four resistors ($R_1 \sim R_4$) are practically equal and that the relative resistance changes are small with $\Delta R_i/R_i << 1$ ($i = 1 \sim 4$), the total output signal V_{out} of the Wheatstone bridge can be approximated by:

$$V_{\mathrm{out}} = \frac{V_{\mathrm{B}}}{4}\left(\frac{\Delta R_1}{R_1} - \frac{\Delta R_2}{R_2} + \frac{\Delta R_3}{R_3} - \frac{\Delta R_4}{R_4}\right) \tag{4.3.3}$$

where V_{B} is a bias voltage of the Wheatstone bridge. Thus, if the sign of the resistance changes ΔR_1 and ΔR_3 are opposite to those of ΔR_2 and ΔR_4, the full Wheatstone bridge yields an amplification of another factor of 4. If we configure the MSS structure (i.e., membrane-type structure), this condition is fulfilled since the dominant stresses induced on the membrane are σ_x in R_1, R_3, and σ_y in R_2, R_4, resulting in opposite signs for the relative resistance changes in each set of resistors. Therefore, the whole induced surface stress is efficiently utilized, and thus MSS realizes the following properties: high sensitivity, self-compensating low-drift operation with full Wheatstone bridge, and stable operation without a free end.

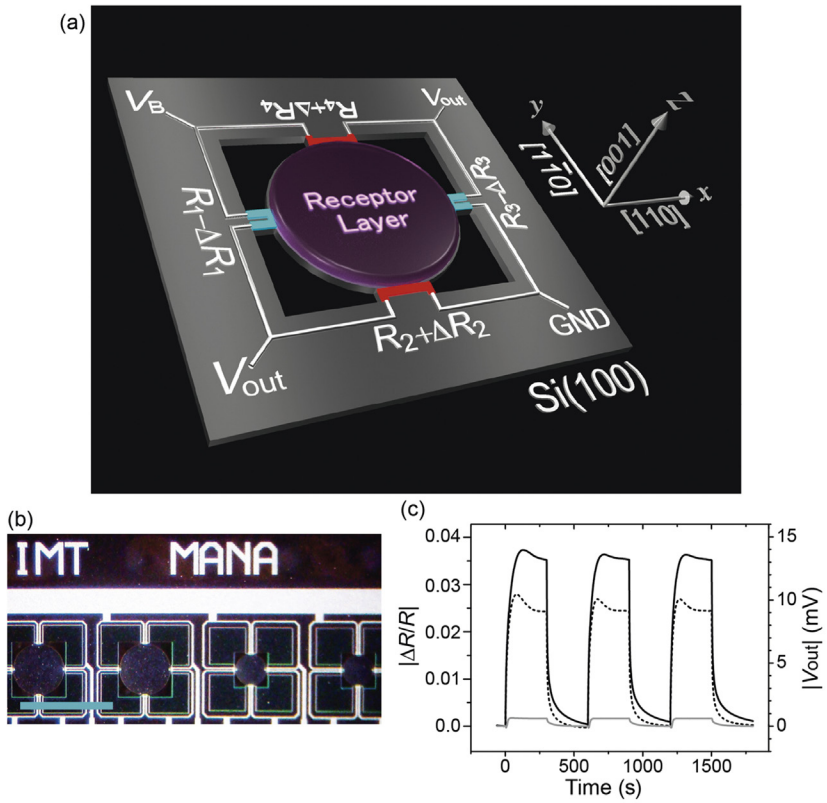

FIGURE 4.3.5 (a) Schematic illustration of a MSS with the configuration of typical electrical wirings. The whole surface stress induced on the round center membrane is efficiently detected by piezoresistors embedded in the constricted beams. (b) Photo of membranes aligned in a fabricated MSS chip. Scale bar corresponds to 1 mm. Membranes with diameters of 500 and 300 μm are fabricated in the same chip to examine the size dependence under the same condition. (c) Output signals (V_{out}) and corresponding values of $|\Delta R/R|$ obtained by the MSS having a diameters of 500 μm (solid line) and 300 μm (dashed line), and by a standard piezoresistive cantilever (gray line). Significant enhancement in sensitivity is confirmed in addition to the size dependence of MSS. *Reproduced from Ref. [10], with permission from the Royal Society of Chemistry.*

4.3.3 Functionalization of Nanomechanical Sensors

In this section, we focus on the fabrication of receptor layers. Nanomechanical sensors are usually coated with various kinds of materials, so-called "receptor layers," where analytes are captured. The adsorbed/absorbed analytes then cause surface stress, which results in the deflection of nanomechanical sensing units. Therefore, the sensing features depend on the quality of the coating (i.e., surface roughness, a coffee ring, etc.) as well as physical/chemical properties of receptor layers. A major factor that affects the quality of the coating is a coating method. Thus, we briefly review common coating techniques for the functionalization of nanomechanical sensors. Effects of the coating quality will be discussed using

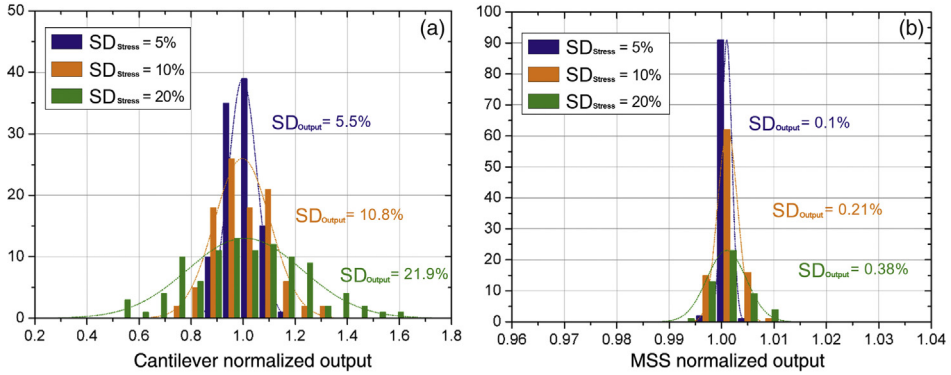

FIGURE 4.3.6 Sensor output distributions of 100 simulated cantilevers (a) and a MSS (b) while a randomly distributed surface stress is applied on their surfaces. *Reprinted from Ref. [34], with permission from Elsevier B.V.*

a cantilever and MSS, focusing on reproducibility of measurements. We also show guidelines to design receptor layers; the structural optimization strategy for high sensitivity.

4.3.3.1 Coating of Receptor Layers

4.3.3.1.1 Reproducibility

Constant sensing performance is a crucial factor for the manufacture of sensors. Loizeau et al. investigated the reproducibility of MSS comparing with a typical cantilever-based sensor [34]. For the practical coating methods such as inkjet spotting and spray coating, the coated receptor layer has a certain amount of roughness in thickness. Such roughness causes inhomogeneous surface stress on the sensors. The stability of the sensing signals for such inhomogeneous surface stress is investigated by means of finite element analysis (FEA), and the results are also confirmed experimentally [34].

The surface stress simulation was conducted for both the cantilever-based sensor and MSS. The surface stress of 0.2 N/m was nonuniformly applied to the sensors with the standard deviation of 5, 10, and 20%. One hundred cases were simulated for each sensor. Figure 4.3.6 shows the distribution of the output signals. In the case of the cantilever-based sensor, the distribution of the output signals had almost the same standard deviations as the surface stress. On the other hand, the standard deviations of the output signals dramatically decreased for the MSS; approximately 50 times smaller than the standard deviations of the surface stress. These results indicate that the MSS has a higher stability for the inhomogeneous surface stress compared to a cantilever-based sensor. As the inhomogeneous surface stress is mainly caused by the roughness of the receptor layers, these results suggest that the MSS is less influenced by the quality of the coatings, leading to the higher uniformity of the sensing performance. The results of the FEA simulations were also confirmed experimentally (Fig. 4.3.7). On the basis of the FEA simulation and the experimental results, the higher reproducibility of the MSS compared to a cantilever-based sensor was demonstrated; the output signal of the MSS is less influenced by the

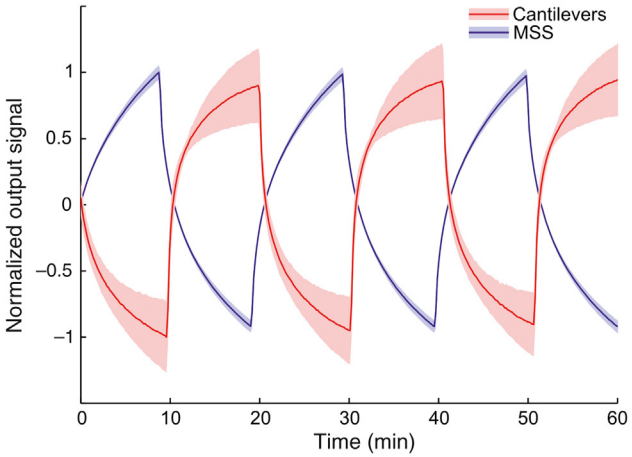

FIGURE 4.3.7 Normalized dynamic responses of 8 cantilevers and 15 MSSs to humidity pulses between 0% and 5%. Solid lines represent average curves and shaded zones highlight standard deviations. Note that the opposite signs of output signals of cantilevers and MSS are due to the opposite directions of stresses on the piezoresistors. *Reprinted from Ref. [34] with permission from Elsevier B.V.*

roughness of the receptor layer. This enhanced sensor-to-sensor repeatability leads not only to accurate and reliable data acquisition in research, but also to the mass production of nanomechanical sensors.

4.3.3.1.2 Double-Side Coating

One of the important challenges of nanomechanical sensors is how to prepare receptor layers in a reproducible manner without any complicated apparatus. Drop casting and dip-coating are examples of fast and convenient coating methods. These methods, however, lead to coatings on both sides. In the case of a cantilever-based sensor with the optical (laser) readout method, the double-side coating does not work because the cantilever does not have measurable vertical deformation as shown in Fig. 4.3.8b. In contrast to the optical readout case, signals are obtained with a double-side-coated piezoresistive cantilever sensor [35,36]. An in-plane elongation caused by the surface stresses on both sides can be detected by the piezoresistor embedded at the clamped end (Fig. 4.3.8d). However, only a local stress induced at the surface where the piezoresistor is embedded can be detected, leading to low sensitivity. Taking account of the conventional cantilever-type geometry and the material property of silicon, it is difficult to realize high sensitivity with the double-side coating.

The MSS geometry is an effective solution to overcome this issue [5]. The in-plane stress induced in the membrane can be detected at the four beams. Figures 4.3.8g and h are the results of FEA simulations on the MSS structure. A surface stress of –3.0 N/m is uniformly applied only on the top surface (Fig. 4.3.8g) or both sides (Fig. 4.3.8h). The distribution of the relative resistance change ($\Delta R/R$) is presented by light and shade. Large relative resistance changes can be observed for the single-side-coated MSS [3]. Although the signal is not as large as the single-side-coated MSS, the

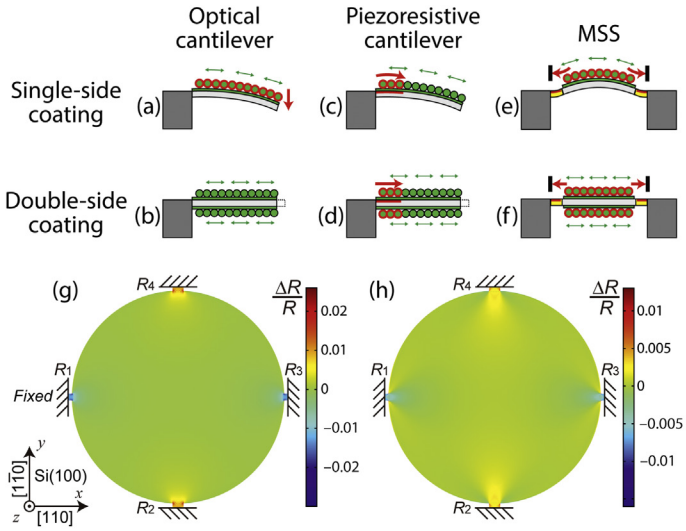

FIGURE 4.3.8 Schematic side views of (a, b) optical and (c, d) piezoresistive cantilevers and (e, f) a MSS with single- and double-side coatings, respectively. FEA of the distribution of $\Delta R/R$ in the middle plane (150 nm below the top surface) of the piezoresistors. A surface stress of −3.0 N/m is applied uniformly on (g) the top surface and (h) on both the top and bottom surfaces of the center circular membranes. *Reprinted from Ref. [5], with permission from the American Chemical Society.*

double-side-coated MSS also exhibits notable relative resistance changes. The double-side-coated MSS yields approximately 37% of the relative resistance change observed with the single-side-coated MSS.

To demonstrate the feasibility of the double-side coating method, the MSS membrane was functionalized by simply dipping it into an aqueous solution containing polyvinyl-pyrrolidone (PVP). Figure 4.3.9a shows a photograph of a simple hand-operated dipping process. An MSS chip was dipped into the PVP aqueous solution, and then dried in air. The coated MSS was used to measure water vapor. Fig. 4.3.9b shows the results of the measurements. Sufficient signal outputs are obtained with a good reproducibility. Such consistent signals from different channels would compensate the decreased sensitivity compared to the single-side-coated MSS because consistent signals from N channels improve the signal-to-noise ratio by a factor of $N^{1/2}$.

4.3.3.2 Guideline to the Design of Receptor Layers

4.3.3.2.1 Thickness

According to a recent study [11], deflection (signal intensity) of a nanomechanical sensor strongly depends on the thickness of a receptor layer. In this section, we focus on the analytical model that describes the relationship between deflection of a cantilever and various physical parameters of a cantilever itself and receptor layer on it. This analysis provides a practical guideline to optimize the thickness of a receptor layer.

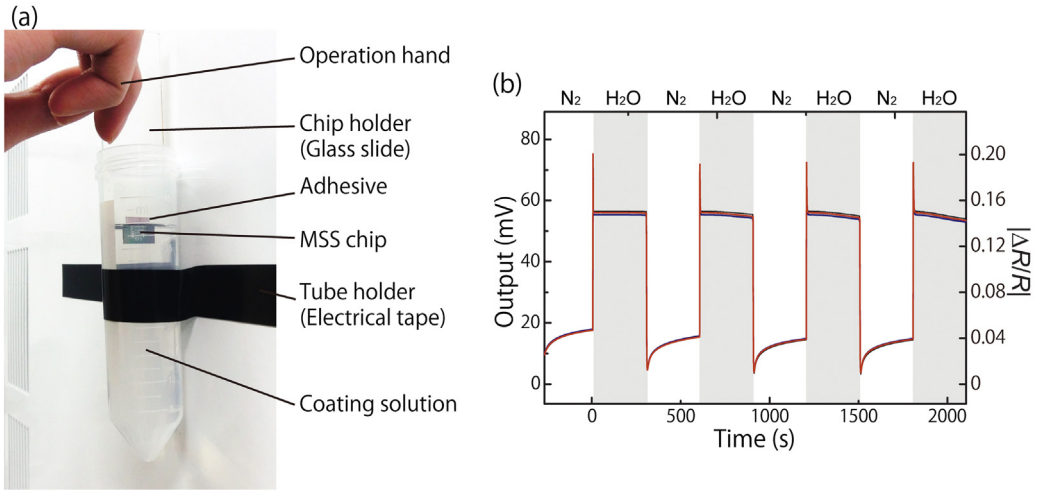

FIGURE 4.3.9 (a) Photograph of the hand-operated dip coating setup for creating double-sided coatings for the MSS chip. (b) Obtained output signals (V_{out}) for three MSS membranes on the same double-side-coated chip. This MSS chip was coated with PVP using hand-operated dip coating. *Reprinted from Ref. [5], with permission from the American Chemical Society.*

The Stoney's equation is widely used to estimate the deflection of a cantilever [37]. According to the Stoney's equation, the deflection of a cantilever (Δz) caused by surface stress (σ_{surf}) is written as:

$$\Delta z = \frac{3(1-\nu_c)l_c^2}{E_c t_c^2}\sigma_{surf} \tag{4.3.4}$$

where E_c and ν_c are the Young's modulus and Poisson's ratio, and l_c and t_c correspond to the length and thickness of a cantilever, respectively. Although this equation has been widely used, no parameters relating to a receptor layer are included. It leads to a large discrepancy for a cantilever with a relatively thick receptor layer.

To consider the effect of a receptor layer, Timoshenko beam theory, which was originally developed to analyze a bimetal strip, can be used [38]. Based on the Timoshenko beam theory, an analytical model for the static deflection of a cantilever sensor coated with a solid layer was derived. In a simple cantilever coated with a solid receptor layer as shown in Fig. 4.3.10, the deflection of the cantilever is described as:

$$\Delta z = \frac{3l^2(t_f + t_c)}{(A+4)t_f^2 + (A^{-1}+4)t_c^2 + 6t_f t_c}\varepsilon_f \tag{4.3.5}$$

$$A = \frac{E_f w_f t_f (1-\nu_c)}{E_c w_c t_c (1-\nu_f)}, \tag{4.3.6}$$

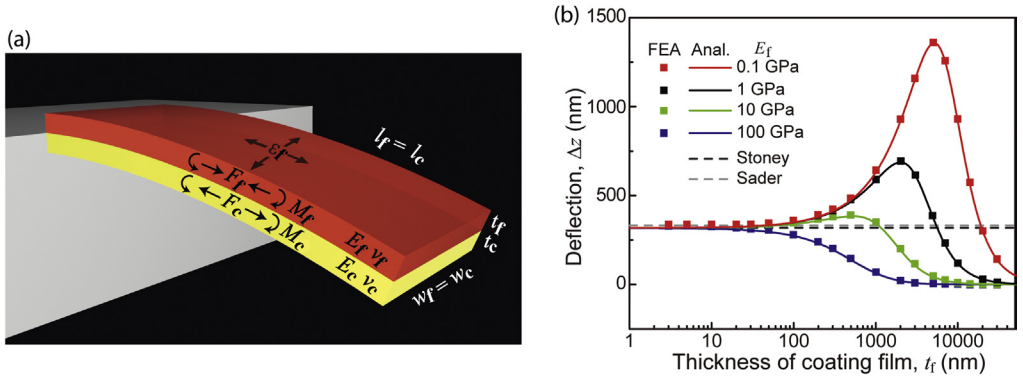

FIGURE 4.3.10 (a) Schematic illustration of a cantilever covered by a coating film with isotropic internal strain. (b) Dependence of cantilever deflection on the thickness of coating films with various Young's moduli from 0.1 GPa to 100 GPa. The values calculated by FEA are represented with filled squares. Black and gray dashed lines correspond to the cantilever deflection calculated by the Stoney's equation and Sader's model, respectively. l = 500 μm, $w_c = w_f$ = 100 μm, t_c = 1 μm, E_c = 170 GPa, ν_c = 0.28, ν_f = 0.30, and σ_{surf} = 0.1 N/m. *Reprinted from Ref. [11], with permission from the American Institute of Physics.*

where E_f, ν_f, and t_f are the Young's modulus, the Poisson's ratio, and the thickness of a receptor layer, and w_c and w_f are the width of a cantilever and a receptor layer, respectively. By replacing the strain of a coating film (ε_f) using the relations $\varepsilon_f = \sigma_f (1 - \nu_f)/E_f$ or $\sigma_f = \sigma_{surf}/t_f$, the deflection of a cantilever (Δz) can be described as a function of internal stress in the receptor layer (σ_f) or surface stress (σ_{surf}). In the case of $t_c \gg t_f$ and $w_c = w_f$, Eq. (4.3.5) reduces to the Stoney's equation.

To verify this analytical result, FEA simulation was also performed for a cantilever with the same geometry. The results are shown in Fig. 4.3.10b. The values obtained from the FEA simulation show a good agreement with the analytically derived curves. The Stoney's model and Sader's model are also drawn in Fig. 4.3.10b, both of which show significant deviations from the FEA analysis [39].

The thickness of a receptor layer can be optimized based on Eq. (4.3.5). The deflection reaches maximum at $t_{t\text{-}op}$, at which $d\Delta z/dt$ becomes zero. In the case of $w_c = w_f$, $t_{t\text{-}op}$ can be written as:

$$t_{t\text{-}op} = \frac{t_c}{2}\left(X^{1/3} + X^{-1/3} - 1\right) \tag{4.3.7}$$

$$X = \frac{2U_c - U_f - 2\sqrt{U_c\left(U_c - U_f\right)}}{U_f} \tag{4.3.8}$$

where $U_c = E_c(1 - \nu_f)$ and $U_f = E_f(1 - \nu_c)$. Thus, one can easily find the optimum thickness of a receptor layer by using Eqs. (4.3.7) and (4.3.8).

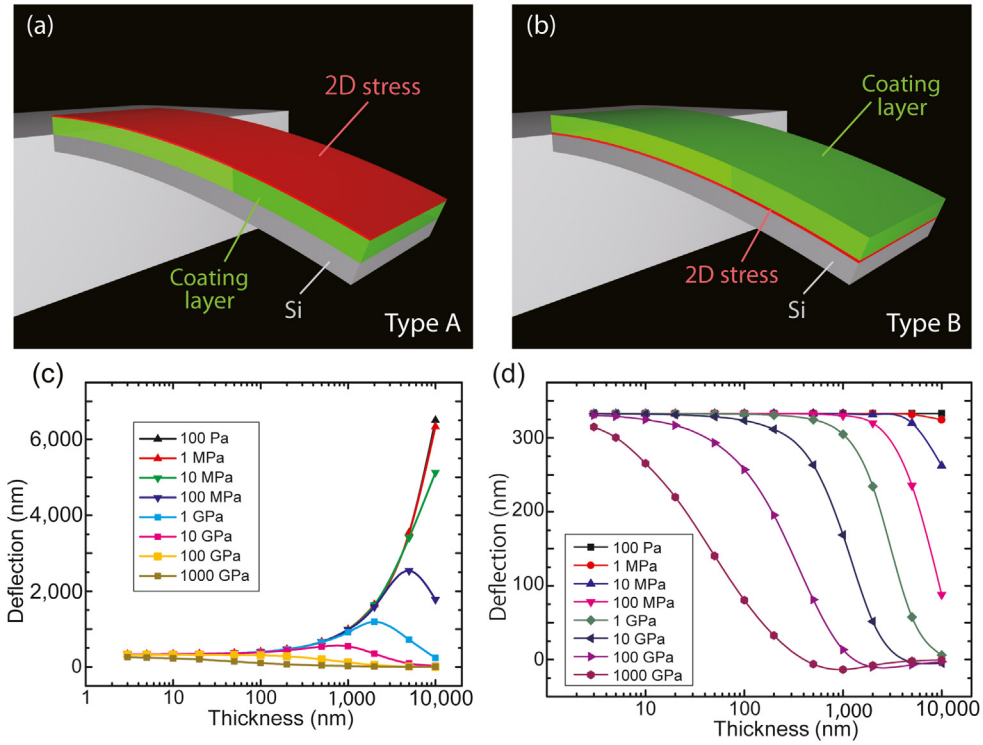

FIGURE 4.3.11 (a) Visualization of the two systems of two-dimensional stress induced on a cantilever-type nanomechanical sensor. (a) Type A system in which the stress is induced on the top surface of the coating layer. (b) Type B system in which the stress is induced at the interface between the silicon cantilever and the coating layer. Note that the dimensions and deflections of the cantilever and the coating layer are exaggerated. Thickness dependence on the deflection of the cantilever in the case of (c) Type A and (d) Type B. Poisson's ratio of coating layers is 0.30 for all plots. *Reprinted from Ref. [12], with permission from the American Scientific Publishers.*

4.3.3.2.2 Configuration

Analytes adsorbed/absorbed on a cantilever sensor can induce two-dimensional stress on the surface of the receptor layer (type A) or on the interface between the receptor layer and the cantilever (type B) as depicted in Fig. 4.3.11. The type A stress is induced when the surface of a cantilever is modified by functional groups including self-assembled monolayers. Analytes that induce charge distribution at the interface by dipole interactions can cause the type B stress. Here, we focus on these two cases [12].

The deflection of a cantilever sensor is investigated by FEA simulation. The length, width, and thickness of the cantilever are set at 500, 100, and 1 μm, respectively. The results are depicted in Fig. 4.3.11c and d. The deflection is plotted as a function of thickness. As we have seen in the previous section, the deflection increases by decreasing the Young's modulus for the type A stress. There is an optimal thickness $t_{\text{t-op}}$ written as Eq. (4.3.7). The

type B stress gives rise to even lower deflections compared to the type A stress. In contrast to the type A, the deflection monotonically decreases with increasing thickness regardless of Young's modulus.

4.3.4 Nanomechanical Sensing of Biomolecules

Detection of biomolecules is an important issue in various fields. For example, detection of biomarkers for cancer in an early stage could significantly reduce the mortality of the patients. Detection of glucose in blood enables us to monitor the blood sugar level, which is essential for diagnosis of diabetes. Biosensors that can detect infectious viruses in real time with high sensitivity are highly required with regard to the control of epidemics. In fundamental science, detection of physical forces generated by a single cell or a number of cells, which are known to show collective motion, is a major challenge to investigate various stimuli-responsive behaviors of cells. Here, we focus on the sensing techniques for biomolecules using nanomechanical sensors. First, we give an overview of previous nanomechanical sensing studies related to the detection of biomolecules. Then, we describe the nanomechanical approach to detect cellular forces.

4.3.4.1 General

Many biomolecules and microorganisms have been detected by means of nanomechanical sensors. Table 4.3.1 summarizes the reported studies [40]. Molecular recognition techniques play an important role in biosensing applications. Antigen–antibody interaction is one of the most powerful tools to detect biomolecules, making it possible to detect targets with high sensitivity and selectivity. Not only peptides including antigens and antibodies themselves, but also microorganisms such as viruses and fungi can be detected by antigen–antibody binding. Another promising technique to detect biomolecules is enzyme reactions. Enzyme reactions can be applied to detect smaller biomolecules such as hydrogen peroxide and glucose.

4.3.4.2 Cells

Mechanobiology is a discipline at the interface of biology and engineering [88]. It focuses on how cells or tissues respond to mechanical stimuli. Since some diseases are known to closely correlate with mechanical changes in cellular systems, advances in mechanobiology lead to the development of mechanical therapies. Moreover, it is reported that biomechanical forces trigger stem cell differentiation, implying its possible control [89]. Thus, mechanobiology has a great potential for the discovery of fundamental biological concepts as well as the development of mechanical therapies.

To investigate the mechanics in cellular systems, measuring the mechanical properties of living cells such as Young's modulus, surface tension, and force distribution is an important

Table 4.3.1 Reported Studies of the Many Biomolecules and Microorganisms that have been Detected by Means of Nanomechanical Sensors [40]

Analytes	References
Glucose	[41–44]
Fructose	[45]
Hydrogen peroxide	[46–48]
α-Amino acid and peptides	[49,50]
Acetylcholine	[47]
Lipid bilayer	[51]
Myoglobin	[52,53]
C-reactive protein	[54–56]
Bovine serum albumin	[57]
Human serum albumin	[58,59]
Human growth hormone	[60]
Protein kinase	[61]
Prostate-specific antigen	[62–64]
Single-chain Fv	[65]
Cytokine	[66]
Human estrogen receptor protein	[67]
Low density lipoproteins	[68]
Cyclin-dependent protein kinase	[69]
Human epidermal growth factor receptor 2	[70]
Immunoglobulin G	[57,71]
Alpha-fetoprotein	[72
Human immunodeficiency virus	[72]
Vaccinia virus	[74]
Bacterial virus T5	[75]
Severe acute respiratory syndrome associated coronavirus	[76]
A. niger	[77]
Bacillus anthracis	[78–80]
Enterohemorrhagic *Escherichia coli* serotype	[81–84]
Salmonella typhimurium	[85]
Tularemia	[86]
Cryptosporidium	[87]

challenge [90]. Nanomechanical sensors have a distinct advantage over measuring the mechanical properties of cellular systems as the principle of nanomechanical sensors is based on the detection of strain/stress and the resultant deflection. Maloney et al. reported the monitoring of single *Aspergillus niger* spore growth by means of functionalized cantilevers [91]. They detected the growth of single spores as changes in resonant frequency. It has been reported by Bischofs et al. that cell migration causes surface tension of ~2 mN/m, which is larger than the detection limit of the nanomechanical sensors with high sensitivity, such as optical readout cantilevers (typically 0.15–0.90 mN/m) and MSS (<0.1 mN/m) [3]. Thus, nanomechanical sensors would provide new grounds for exploring the mechanical properties of living cells.

4.3.5 Conclusions and Future Trends

In this chapter, we briefly overviewed the basics of nanomechanical sensing, focusing on the working principles and representative readout methods. Then, we reviewed a recently developed nanomechanical sensing platform; MSS, which has various practical advantages over conventional nanomechanical sensors. The analytical approach to designing a receptor layer with optimized sensitivity was explained. Since they can detect volume and/or mass of analytes, nanomechanical sensors are promising devices for the measurements of diverse biomaterials, ranging from small molecules (e.g., volatile organic compounds, amino acid) to microorganisms (e.g., viruses, cells) as summarized in this chapter. In addition, application of nanomechanical sensors to mechanobiology, an emerging field of science, would provide new biological concepts; clarifying the mechanics in cellular systems and mechanical basis of tissue regulation.

References

[1] N.V. Lavrik, M.J. Sepaniak, P.G. Datskos, Rev. Sci. Instrum. 75 (2004) 2229.

[2] K.R. Buchapudi, X. Huang, X. Yang, H.-F. Ji, T. Thundat, Analyst 136 (2011) 1539.

[3] G. Yoshikawa, T. Akiyama, S. Gautsch, P. Vettiger, H. Rohrer, Nano Lett. 11 (2011) 1044.

[4] G. Yoshikawa, T. Akiyama, F. Loizeau, K. Shiba, S. Gautsch, T. Nakayama, P. Vettiger, N.F. de Rooij, M. Aono, Sensors 12 (2012) 15873.

[5] G. Yoshikawa, F. Loizeau, C.J.Y. Lee, T. Akiyama, K. Shiba, S. Gautsch, T. Nakayama, P. Vettiger, N.F. de Rooij, M. Aono, Langmuir 29 (2013) 7551.

[6] J.K. Gimzewski, C. Gerber, E. Meyer, R.R. Schlittler, Chem. Phys. Lett. 217 (1994) 589.

[7] T. Thundat, R.J. Warmack, G.Y. Chen, D.P. Allison, Appl. Phys. Lett. 64 (1994) 2894.

[8] R. Berger, E. Delamarche, H.P. Lang, C. Gerber, J.K. Gimzewski, E. Meyer, H.J. Guntherodt, Science 276 (1997) 2021.

[9] J. Fritz, M.K. Baller, H.P. Lang, H. Rothuizen, P. Vettiger, E. Meyer, H.J. Guntherodt, C. Gerber, J.K. Gimzewski, Science 288 (2000) 316.

[10] G. Yoshikawa, Nanomechanical sensors and membrane-type surface stress sensor (MSS) for medical, security and environmental applications, Manipulation of Nanoscale Materials: An Introduction to Nanoarchitectonics, The Royal Society of Chemistry, Burlington House, London, UK, (2012) pp. 428.

[11] G. Yoshikawa, Appl. Phys. Lett. 98 (2011) 173502.

[12] G. Yoshikawa, C.J.Y. Lee, K. Shiba, J. Nanosci. Nanotechnol. 14 (2014) 2908.

[13] A. Bietsch, J.Y. Zhang, M. Hegner, H.P. Lang, C. Gerber, Nanotechnology 15 (2004) 873.

[14] S.M. Heinrich, M.J. Wenzel, F. Josse, I. Dufour, J. Appl. Phys. 105 (2009) 124903.

[15] Y.T. Yang, C. Callegari, X.L. Feng, K.L. Ekinci, M.L. Roukes, Nano Lett. 6 (2006) 583.

[16] M. Li, H.X. Tang, M.L. Roukes, Nat. Nanotechnol. 2 (2007) 114.

[17] T. Braun, V. Barwich, M.K. Ghatkesar, A.H. Bredekamp, C. Gerber, M. Hegner, H.P. Lang, Phys. Rev. E 72 (2005) 031907.

[18] M.K. Ghatkesar, V. Barwich, T. Braun, J.P. Ramseyer, C. Gerber, M. Hegner, H.P. Lang, U. Drechsler, M. Despont, Nanotechnology 18 (2007) 445502.

[19] M.K. Ghatkesar, T. Braun, V. Barwich, J.P. Ramseyer, C. Gerber, M. Hegner, H.P. Lang, Appl. Phys. Lett. 92 (2008).

[20] A.W. McFarland, M.A. Poggi, M.J. Doyle, L.A. Bottomley, J.S. Colton, Appl. Phys. Lett. 87 (2005) 053505.

[21] M.J. Lachut, J.E. Sader, Phys. Rev. Lett. 99 (2007) 206102.

[22] M.J. Lachut, J.E. Sader, Appl. Phys. Lett. 95 (2009) 193505.

[23] D. Lee, S. Kim, N. Jung, T. Thundat, S. Jeon, J. Appl. Phys. 106 (2009) 024310.

[24] L. Aeschimann, A. Meister, T. Akiyama, B.W. Chui, P. Niedermann, H. Heinzelmann, N.F. De Rooij, U. Staufer, P. Vettiger, Microelectron. Eng. 83 (2006) 1698.

[25] J.H. He, Y.F. Li, J. Phys. 34 (2006) 429.

[26] X.M. Yu, Y.Q. Tang, H.T. Zhang, T. Li, W. Wang, IEEE Sens. J. 7 (2007) 489.

[27] N.L. Privorotskaya, W.P. King, Microsyst. Technol. 15 (2008) 333.

[28] F.T. Goericke, W.P. King, IEEE Sens. J. 8 (2008) 1404.

[29] A. Loui, F.T. Goericke, T.V. Ratto, J. Lee, B.R. Hart, W.P. King, Sensors Actuat. A. 147 (2008) 516.

[30] Y. Kanda, IEEE Trans. Electron. Devices 29 (1982) 64.

[31] W.G. Pfann, R.N. Thurston, J. Appl. Phys. 32 (1961) 2008.

[32] Y. Kanda, Sensors Actuat. A 28 (1991) 83.

[33] P.A. Rasmussen, O. Hansen, A. Boisen, Appl. Phys. Lett. 86 (2005) 203502.

[34] F. Loizeau, T. Akiyama, S. Gautsch, P. Vettiger, G. Yoshikawa, N.F. de Rooij, Sensors Actuat. A 228 (2015) 9.

[35] P.A. Rasmussen, A.V. Grigorov, A. Boisen, J. Micromech. Microeng. 15 (2005) 1088.

[36] A. Choudhury, P.J. Hesketh, T.G. Thundat, H. Zhiyu, R. Vujanic, Design and testing of single and double sided cantilevers for chemical sensing, Sensors, 2007 IEEE 1–3 (2007) 1432.

[37] G.G. Stoney, Proc. R. Soc. Lond. Ser. A 82 (1909) 172.

[38] S. Timoshenko, J. Opt. Soc. Am. 11 (1925) 233.

[39] J.E. Sader, J. Appl. Phys. 89 (2001) 2911.

[40] K.R. Buchapudi, X. Huang, X. Yang, H.F. Ji, T. Thundat, Analyst. 136 (2011) 1539.

[41] A. Subramanian, P.I. Oden, S.J. Kennel, K.B. Jacobson, R.J. Warmack, T. Thundat, M.J. Doktycz, Appl. Phys. Lett. 81 (2002) 385.

[42] J. Pei, F. Tian, T. Thundat, Anal. Chem. 76 (2004) 292.

[43] T. Chen, D.P. Chang, T. Liu, R. Desikan, R. Datar, T. Thundat, R. Berger, S. Zauscher, J. Mater. Chem. 20 (2010) 3391.

[44] X. Huang, S. Li, J.S. Schultz, Q. Wang, Q. Lin, Sensors Actuat. B 140 (2009) 603.

[45] G.A. Baker, R. Desikan, T. Thundat, Anal. Chem. 80 (2008) 4860.

[46] X.D. Yan, X.L. Shi, K. Hill, H.F. Ji, Anal. Sci. 22 (2006) 205.

[47] H. Gao, K.R. Buchapudi, A. Harms-Smyth, M.K. Schulte, X. Xu, H.-F. Ji, Langmuir 24 (2008) 345.

[48] J.P. Lock, E. Geraghty, L.C. Kagumba, K.K. Mahmud, Thin Solid Films 517 (2009) 3584.

[49] P. Dutta, C.A. Tipple, N.V. Lavrik, P.G. Datskos, H. Hofstetter, O. Hofstetter, M.J. Sepaniak, Anal. Chem. 75 (2003) 2342.

[50] B.H. Kim, O. Mader, U. Weimar, R. Brock, D.P. Kern, J. Vac. Sci. Technol. B 21 (2003) 1472.

[51] I. Pera, J. Fritz, Langmuir 23 (2007) 1543.

[52] Y. Arntz, J.D. Seelig, H.P. Lang, J. Zhang, P. Hunziker, J.P. Ramseyer, E. Meyer, M. Hegner, C. Gerber, Nanotechnology 14 (2003) 86.

[53] G.Y. Kang, G.Y. Han, J.Y. Kang, I.-H. Cho, H.-H. Park, S.-H. Paek, T.S. Kim, Sensors Actuat. B 117 (2006) 332.

[54] J.H. Lee, K.H. Yoon, K.S. Hwang, J. Park, S. Ahn, T.S. Kim, Biosens. Bioelectron. 20 (2004) 269.

[55] T.Y. Kwon, K. Eom, J.H. Park, D.S. Yoon, T.S. Kim, H.L. Lee, Appl. Phys. Lett. 90 (2007) 223903.

[56] K.W. Wee, G.Y. Kang, J. Park, J.Y. Kang, D.S. Yoon, J.H. Park, T.S. Kim, Biosens. Bioelectron. 20 (2005) 1932.

[57] A.M. Moulin, S.J. O'Shea, R.A. Badley, P. Doyle, M.E. Welland, Langmuir 15 (1999) 8776.

[58] S. Stolyarova, S. Cherian, R. Raiteri, J. Zeravik, P. Skladal, Y. Nemirovsky, Sensors Actuat. B 131 (2008) 509.

[59] G.A. Campbell, R. Mutharasan, Anal. Chem. 78 (2006) 2328.

[60] M. Calleja, J. Tamayo, M. Nordström, A. Boisen, Appl. Phys. Lett. 88 (2006) 113901.

[61] H.-S. Kwon, K.-C. Han, K.S. Hwang, J.H. Lee, T.S. Kim, D.S. Yoon, E.G. Yang, Anal. Chim. Acta 585 (2007) 344.

[62] G.H. Wu, R.H. Datar, K.M. Hansen, T. Thundat, R.J. Cote, A. Majumdar, Nat. Biotechnol. 19 (2001) 856.

[63] C. Vancˇura, Y. Li, J. Lichtenberg, K.-U. Kirstein, A. Hierlemann, F. Josse, Anal. Chem. 79 (2007) 1646.

[64] S.M. Lee, K.S. Hwang, H.J. Yoon, D.S. Yoon, S.K. Kim, Y.S. Lee, T.S. Kim, Lab Chip 9 (2009) 2683.

[65] N. Backmann, C. Zahnd, F. Huber, A. Bietsch, A. Pluckthun, H.P. Lang, H.J. Güntherodt, M. Hegner, C. Gerber, Proc. Natl. Acad. Sci. USA 102 (2005) 14587.

[66] P. Dutta, J. Sanseverino, P.G. Datskos, M.J. Sepaniak, Nanobiotechnology 1 (2005) 237.

[67] R. Mukhopadhyay, V.V. Sumbayev, M. Lorentzen, J. Kjems, P.A. Andreasen, F. Besenbacher, Nano Lett. 5 (2005) 2385.

[68] A.M. Moulin, S.J. O'Shea, M.E. Welland, Ultramicroscopy 82 (2000) 23.

[69] W. Tan, Y. Huang, T. Nan, C. Xue, Z. Li, Q. Zhang, B. Wang, Anal. Chem. 82 (2010) 615.

[70] J.A. Capobianco, W.Y. Shih, Q.-A. Yuan, G.P. Adams, W.-H. Shih, Rev. Sci. Instrum. 79 (2008) 076101.

[71] T. Kwon, J. Park, J. Yang, D.S. Yoon, S. Na, C.-W. Kim, J.-S. Suh, Y.-M. Huh, S. Haam, K. Eom, PLoS One 4 (2009) e6248.

[72] Y.J. Liu, X.X. Li, Z.X. Zhang, G.M. Zuo, Z.X. Cheng, H.T. Yu, Biomed. Microdevices 11 (2009) 183.

[73] Y. Lam, N.I. Abu-Lail, M.S. Alam, S. Zauscher, Nanomed. Nanotechnol. Biol. Med. 2 (2006) 222.

[74] R.L. Gunter, W.G. Delinger, K. Manygoats, A. Kooser, T.L. Porter, Sensors Actuat. A 107 (2003) 219.

[75] T. Braun, M.K. Ghatkesar, N. Backmann, W. Grange, P. Boulanger, L. Letellier, H.-P. Lang, A. Bietsch, C. Gerber, M. Hegner, Nat. Nano. 4 (2009) 179.

[76] V. Sreepriya, J. Hai-Feng, Meas. Sci. Technol. 17 (2006) 2964.

[77] N. Nugaeva, K.Y. Gfeller, N. Backmann, M. Duggelin, H.P. Lang, H.J. Guntherodt, M. Hegner, Microsc. Microanal. 13 (2007) 13.

[78] A.P. Davila, J. Jang, A.K. Gupta, T. Walter, A. Aronson, R. Bashir, Biosens. Bioelectron. 22 (2007) 3028.

[79] J.-P. McGovern, W.Y. Shih, R. Rest, M. Purohit, Y. Pandya, W.-H. Shih, Analyst 133 (2008) 649.

[80] L. Fu, S. Li, K. Zhang, Z.-Y. Cheng, MRS Online Proc. Library 951 (2006) E05 04.

[81] J. Zhang, H.F. Ji, Anal. Sci. 20 (2004) 585.

[82] K.Y. Gfeller, N. Nugaeva, M. Hegner, Appl. Environ. Microbiol. 71 (2005) 2626.

[83] J.A. Capobianco, W.Y. Shih, W.-H. Shih, Rev. Sci. Instrum. 77 (2006) 125105.

[84] L. Fu, K. Zhang, S. Li, Y. Wang, T.-S. Huang, A. Zhang, Z.Y. Cheng, Sensors Actuat. B 150 (2010) 220.

[85] Q. Zhu, W.Y. Shih, W.-H. Shih, Biosens. Bioelectron. 22 (2007) 3132.

[86] H.F. Ji, X. Yang, J. Zhang, T. Thundat, Expert Rev. Mol. Diagn. 4 (2004) 859.
[87] G.A. Campbell, R. Mutharasan, Biosens. Bioelectron. 23 (2008) 1039.
[88] T. Mammoto, A. Mammoto, D.E. Ingber, Annu. Rev. Cell Dev. Biol. 29 (2013) 27.
[89] D.A. Lee, M.M. Knight, J.J. Campbell, D.L. Bader, J. Cell. Biochem. 112 (2011) 1.
[90] Z. Xiaoyu Rayne, Z. Xin, J. Micromech. Microeng. 21 (2011) 054003.
[91] N. Maloney, G. Lukacs, J. Jensen, M. Hegner, Nanoscale 6 (2014) 8242.